Available online at www.sciencedirect.com
ScienceDirect
Sensors and Actuators A 132 (2006) 337–345
SENSORS AND ACTUATORS A PHYSICAL
www.elsevier.com/locate/sna

Optimization and fabrication of thick flexible polymer based micro thermoelectric generator

Wulf Glatz *, Simon Muntwyler, Christofer Hierold

Micro and Nanosystems, ETH Zurich, Zurich, Switzerland

Received 23 September 2005; received in revised form 19 March 2006; accepted 11 April 2006
Available online 24 May 2006

Abstract

We present a novel polymer based wafer level fabrication process for micro thermoelectric generators (μTEGs) for the application on non-planar surfaces. The generators are fabricated by subsequent electrochemical deposition (ECD) of Cu and Ni in a 190-μm thick flexible polymer mold formed by photolithographic (PL) patterning of SU-8. First generators were tested and characterized. The TEG generated a power of $12.0 \pm 1.1\,\mathrm{nW/cm^2}$ for a ΔT of 0.12 K at the μTEG interface, which is equivalent to a thermoelectric efficiency factor of $0.83\,\mu\mathrm{W\,K^{-2}\,cm^{-2}}$. The experimental data is in good accordance with a model introduced for the optimization of vertical micro thermoelectric generators. It allows calculation of the optimal geometric design parameters for any given material and thermal interfaces. The analysis reveals that the thermocouple length should be in the range of 80–150 μm when the best thermoelectric bulk material (BiTe) is used and realistic interface condition are assumed.

Keywords: Thermoelectric generator; SU-8; Electrochemical deposition

1. Introduction

Despite all advances in the miniaturization of microsystems most of these systems still depend on a central power source or bulky batteries with limited lifetime. Growing fields like autonomous microsystems or wearable electronics urgently look for microscale power generators. One possible solution is to convert waste heat into electrical power with a thermoelectric generator. A generator driving a wrist watch using a persons body heat has been introduced as a first commercial application [1]. Several other approaches to build TEG by micromachining have been presented.

The standard thin film based michromaching technology constrains the design of such μTEGs. Because of their limited thickness thin film deposited materials have to be laid out rather lateral than vertical inducing thermal losses through the supporting material and limiting the integration density. Placing the thermocouples onto a thin membrane [2] reduces the losses but does not allow for thermally contacting the cold and hot side via the top and bottom surface of the thin device. This might be achieved by either assembly techniques [3,4] which adds to the cost or through the integration of micro cavities underneath the thermocouples [5]. However losses can not be completely avoided, the devices inhibit a relatively high electrical resistance due to the small cross sectional area of the thermocouples and for optimization numerical modeling is required. Recently μTEGs with a vertical set up have been presented [6,7]. Both generators demonstrate the use of BiTe as active material, which is known to be the best thermoelectric material for application around room temperature. Thermocouples with leg length of 20 μm have been deposited by means of electrochemical deposition [6] and sputtering [7]. These generators internal thermal resistances are mainly restricted through the limited thermocouple length. Therefore just a small fraction of the provided temperature difference drops across the thermocouple junctions even if the thermal contact resistances are minimized. In order to operate these generators in their optimum power output range they would have to be fabricated with longer thermocouples.

We introduce a general model to optimize vertical TEGs for material, design and interface parameters. We also present a new truly low cost wafer level process to fabricate μTEGs by subsequent ECD of two different materials in a 190-μm thick polymer mold formed by PL-patterning of the negative resist SU-8. The mold serves as matrix for the final device, which therefore

* Corresponding author.
E-mail address: wulf.glatz@micro.mavt.ethz.ch (W. Glatz).

0924-4247/$ – see front matter © 2006 Elsevier B.V. All rights reserved.
doi:10.1016/j.sna.2006.04.024

is flexible. Flexibility is important to enable the application of these μTEGs on non-planar surfaces.

2. Modeling

Modeling allows the optimization of a TEGs design. Rowe and co-workers [8] showed that for low temperature waste heat applications the design may be optimized for maximum power rather than for coefficient of performance as it is done for thermoelectric cooling devices. The model presented is based on the one proposed by Strasser et al. [5]. A more general approach is chosen and refinements such as consideration of area related electrical and thermal contact resistances are added. The influences of the design parameters on the generator performance are discussed by means of a first level compact analytical model. A general compact model for the actual design optimization is introduced afterwards.

2.1. First level compact model of vertical TEG

The open circuit voltage generated by a thermoelectric generator is proportional to the number of thermocouples m, the relative Seeback coefficient of the used thermocouple materials α and the temperature difference between cold and hot junctions ΔT_G:

$$U_o = m\alpha\Delta T_G \tag{1}$$

The maximum output power P_o is achieved under matched load condition, i.e. the load resistance connected to the generator R_L equals the internal electrical resistance of the generator R_G:

$$P_o = UI = \frac{U_o^2}{4R_G} = \frac{m^2\alpha^2}{4R_G}\Delta T_G^2 \tag{2}$$

where U is the output voltage under load and I is the electrical current. Assuming that the generator is connected to a hot and a cold reservoir via the thermal contact resistances K_C and K_H, respectively as seen in Fig. 1. The temperature drop across the generator ΔT_G may then be expressed as

$$\Delta T_G = \frac{K_G}{K_G + K_C + K_H}\Delta T \tag{3}$$

where K_G is the generators internal thermal resistance and ΔT is the temperature difference between hot and cold reservoir.

Fig. 1 depicts the typical qualitative temperature profile across a TEG with its thermal contact resistances for the two cases of a conventional macroscopic TEG and a μTEG. According to Eq. (2) preferably a big portion of the temperature difference provided by the ambient ΔT should drop across the generator's top and bottom contacts. This condition is fulfilled in the case of the conventional TEG where the thermal resistance of the actual generator K_G is big compared to the interface resistances K_C and K_H.

On the other hand due to fabrication constrains a μTEG is usually a thin device with a low thermal resistance in comparison to the contact resistances even if those are minimal. Increasing the generators internal resistance and minimize the contact resistance is crucial for μTEG development. To allow optimization of

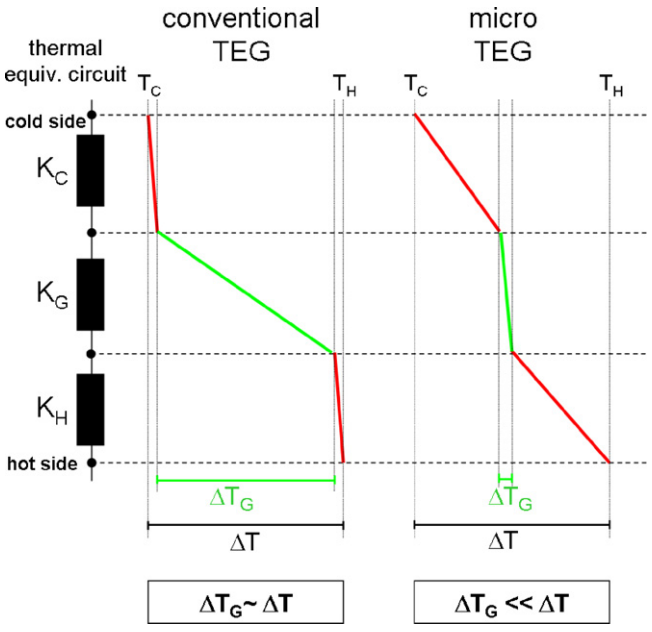

Fig. 1. Thermal equivalent circuit of first level model of TEG and variation of the temperature difference across conventional TEG and μTEG.

μTEGs the thermal examination will be refined and the electrical resistance of the generator will be considered in the following.

Neglecting the effect of any insulating material between the single thermolegs K_G may be expressed as follows:

$$K_G = \frac{l}{2m\lambda_m A_0} \tag{4}$$

where according to Fig. 2 l is the length of the thermocouple, λ_m the mean thermal conductivity of the two thermocouple materials and A_0 is the cross-section area of one thermoleg assuming that both thermolegs do not vary in length and area. The thermal contact resistances to the interfaces are

$$K_C = \frac{k_C}{A_G}; \qquad K_H = \frac{k_H}{A_G} \tag{5}$$

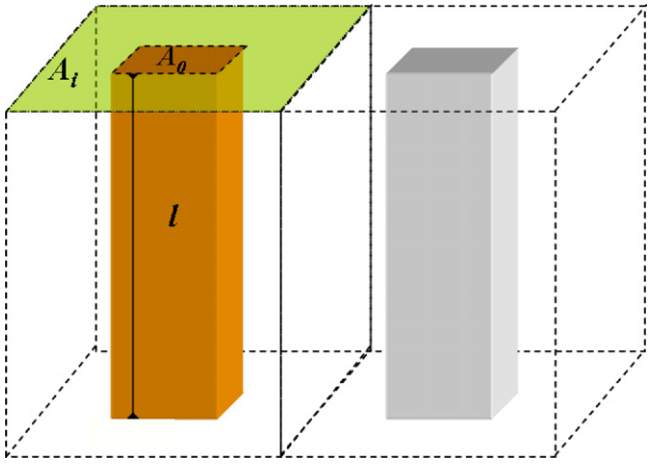

Fig. 2. Thermocouple build of two thermolegs with surrounding insulation material.

where k_C and k_H are the areal thermal contact resistances to the cold and hot side and A_G is the generator surface area. Inserting Eqs. (4) and (5) in Eq. (3) and substituting A_G according to Fig. 2 with $2m(A_0 + A_i)$ the temperature difference across the generator can be expressed as

$$\Delta T_G = \frac{l(1 + A_V)}{l(1 + A_V) + \lambda_m(k_C + k_H)} \Delta T \quad (6)$$

where $A_V = A_i/A_0$ is the ratio of insulating to active area. The generators internal electrical resistance may be approximated by

$$R_G = \frac{2m\rho_m l}{A_0} \quad (7)$$

where ρ_m is the mean electrical resistivity of a thermocouple. In order to compare the performance of different TEGs the output power of the device should be normalized to its surface area and the temperature difference provided to the generator. Hence the figure Φ will be called efficiency factor. The relation for Φ yields from Eqs. (6), (7) and (2):

$$\Phi = \frac{P_o}{A_G \Delta T^2} = \frac{1}{16} \frac{\alpha^2}{\rho_m} \frac{l(1 + A_V)}{(l(1 + A_V) + \lambda_m(k_C + k_H))^2} \quad (8)$$

It can be stated that the power per area depends from three sets of parameters. The material parameters of the thermocouples α, ρ_m, and λ_m, the geometric design parameters l and A_V and the thermal interface related parameters k_C and k_H. The material and thermal interface parameters have a large influence on the generator performance but the following examination will focus on the design parameters, which allow tune the generator to optimum performance for any given material and interfaces. According to Eq. (8) the number of thermocouples and the cross section area of the thermolegs do not influence the generated power per area. Yet the voltage specification of a potential application will determine the necessary number of thermocouples to be integrated on a certain area since according to Eq. (1) the number of thermocouples connected in series defines the voltage output. Fig. 3 shows a plot of the efficiency factor over the thermocouple length. With increasing l the power is initially increasing until it reaches a maximum value and then decreases. For small

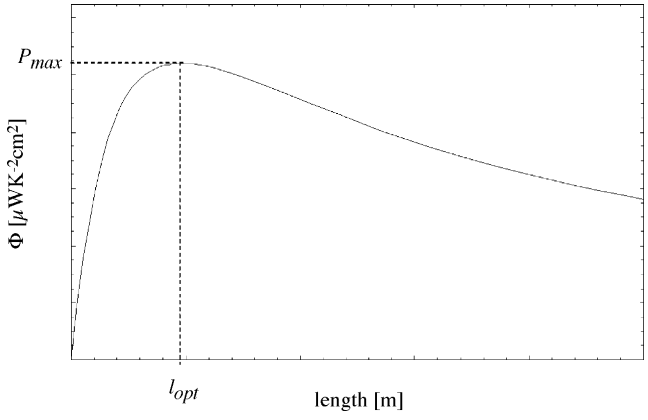

Fig. 3. Thermoelectric efficiency factor over thermocouple length calculated with first level compact model.

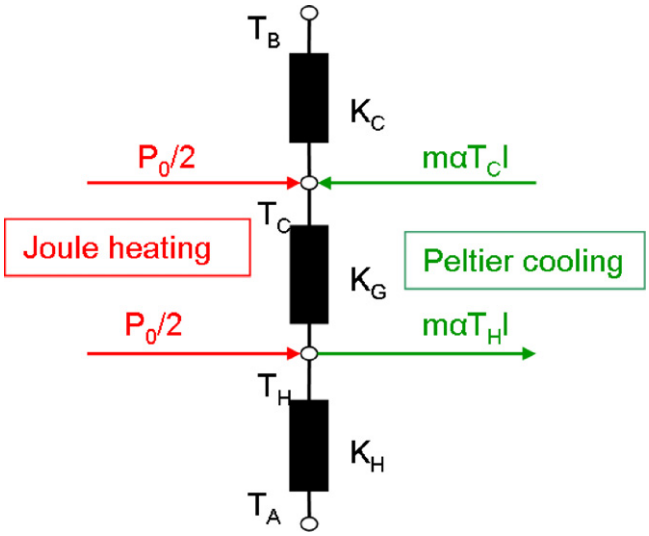

Fig. 4. Thermal equivalent circuit of general model of μTEG.

l the increasing length mainly causes an increase of the ratio $\Delta T_G/\Delta T$ (compare with Eq. (6)). When K_G is in the range of K_C and K_H the negative influence of the length on the internal electric resistance becomes dominant and the power shows a one over l behaviour. As a result the thermocouple length should be chosen such as maximum power is obtained. Solving the equation $(\partial\Phi/\partial l = 0)$ for l yields the optimum length l_{opt}:

$$l_{opt} = \frac{\lambda_m(k_C + k_H)}{(1 + A_V)} \quad (9)$$

Consequently the optimal length is independent of the Seeback coefficient and the electrical resistivty of the thermocouple materials.

2.2. General compact model of vertical TEG

For the actual optimization a general compact model is applied. According to Fig. 4 the model includes Joule heating and Peltier cooling upon flow of an electrical current within the generator. In addition the model considers arbitrary insulation material between the thermocouples and the electrical contact resistance R_C between thermolegs and interconnects. The later is assumed to be inversely proportional to the cross sectional area A_0 of the thermoleg. The Kirchhoff equations, which can be set up from the thermal equivalent circuit, yield to a cubic equation which can be analytically solved as described in [5]. In Fig. 5 the first level and the general compact model are compared. As expected the maximum power P_{max} calculated by the general model is smaller and the optimal length is shifted up because the above mentioned supplements mean additional losses. The first level model yields a first approximation for l_{opt} and P_{max} but obviously for optimization and power estimation the general model should be applied.

Analysis of the dependence of the output power and optimal leg length from the design parameters is performed to determine the fabrication process requirements (see Figs. 6 and 7). The results are summarized in Table 1. Fig. 6 indicates that the regime

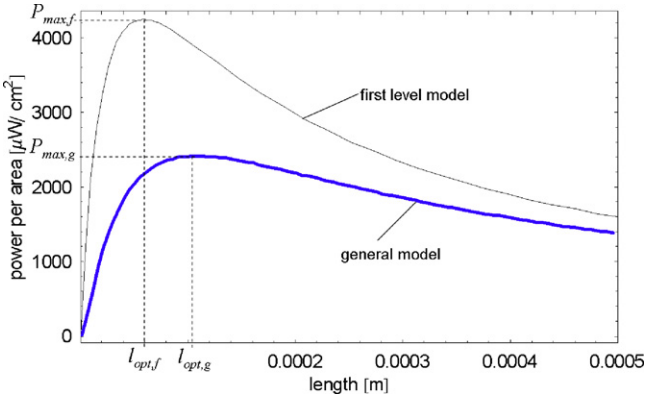

Fig. 5. Comparison of output power over thermocouple length for first level and general model.

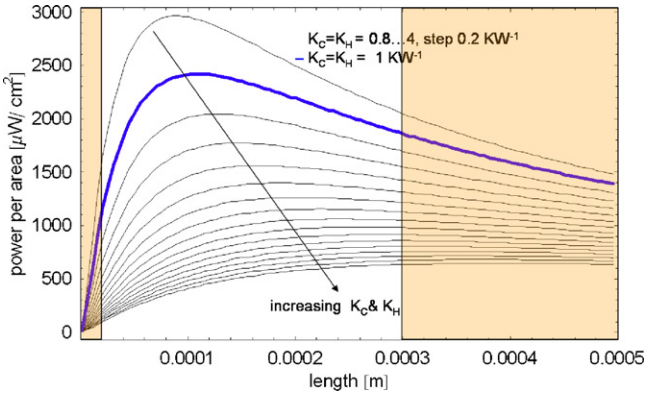

Fig. 6. Output power per area over thermocouple length for variations of thermal contact resistances K_C and K_H. Regimes of conventional and micro fabrications of thermoelectric generators.

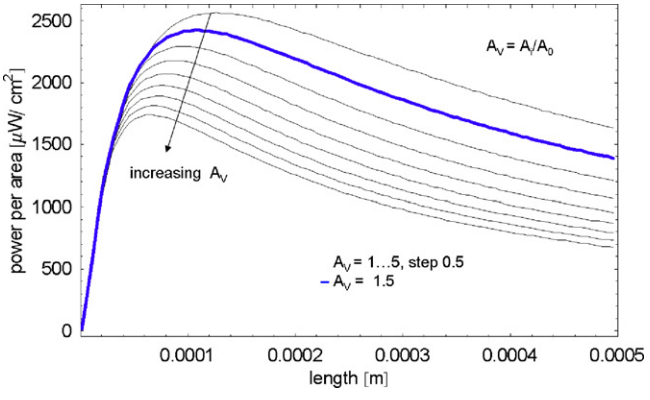

Fig. 7. Output power per area over thermocouple length for variations of A_V.

Table 1
Overview of parameters influences on the maximum power output and the optimal thermocouple length

	P_{max}	l_{opt}
$K_{C,H}$ ↑	↓	↑
A_V ↑	↓	↓
R_C ↑	↓	→

around the maximum performance of the TEG is technologically not yet mastered [9]. Hence a fabrication technology for ideal TEG with thermoleg length from 100 to 200 μm would allow to outperform today's solutions if BiTe is used as thermocouple material.

3. Fabrication

Fig. 8 illustrates the fabrication process flow. The process involves four photolithography steps and four electrochemical deposition steps. A 4 in. Si wafer serves as support for the first process steps and may later be reused. Fig. 8a shows the first photolithography step, which is performed after the deposition of a 300 nm Cu-layer on top of a 4 μm thick polymeric LOR sacrificial layer (MicroChem LOR 30B) that was spun onto the Si wafer. A positive resist (Shipley S 1813) serves as etch mask for the Cu-etch with a sodium persulfate solution. The so defined Cu electrodes serve as seed layer for the ECD of the thermoelectric materials. The two electrodes can then be connected individually at the wafer edge through a customized electroplating chuck with two separate electrodes. Fig. 8b shows the patterning of a 190-μm thick layer of SU-8-50. Etch holes and openings for ECD are aligned to the underlying electrodes. Stress in the SU-8 layer is minimized by ramping both the prebake and the post exposure bake temperature from 50 to 100 °C and from 60 to 95 °C respectively with a rate of 3–4 °C/min [10]. Developing results could be improved with ultrasonic agitation. The first ECD step is illustrated in Fig. 8c. Atop of the connected electrode the copper thermolegs are grown with current controlled cathodic electrochemical deposition (FIBRoplate IKO plating system) in a copper sulphate electrolyte. The other electrode is connected to the cathode potential via a 5 kΩ resistor preventing its dissolution. A deposition rate of 20 μm/h is achieved. In the next step the Ni-thermolegs are deposited as shown in Fig. 8d. The nickel plating is carried out with voltage controlled deposition in a nickel sulfamate bath at 40 °C. The pH value of the bath is kept between 3.5 and 4.1. The deposition rate is 40 μm/h. For both ECD steps square wave current pulses of 10–20 ms are applied to achieve good results in high aspect ratio holes. Any residual unevenness resulting from overgrown metal is removed in a polish step. Fig. 9 shows an array of Cu and Ni columns that were electrochemically deposited into a SU-8 matrix and subsequently polished on a polishing machine (Streuers Abrapohl 2) with silicon carbide paper. One can see small scratches caused by the abrasive particles. Next a 20 μm Cu-layer is electrochemically deposited and then patterned via Cu-etching giving a low-ohmic and mechanically robust connection between the Cu- and Ni-thermolegs (Fig. 8e). The SEM image in Fig. 10 shows a cut through a Ni–Cu thermocouple with a thick Cu interconnect. Because the thermocouples need to be connected in series the electrodes patterned in Fig. 8a have to be replaced by another set of interconnects. For that the SU-8 layer with the embedded thermolegs needs to be released. This is done by removing the LOR with Shipley MF319 developer (Fig. 8f). The LOR is accessed via the etch holes. After flipping the SU-8 disk the plating electrodes become visible. For further processing the released SU-8 disk is bonded to the final package

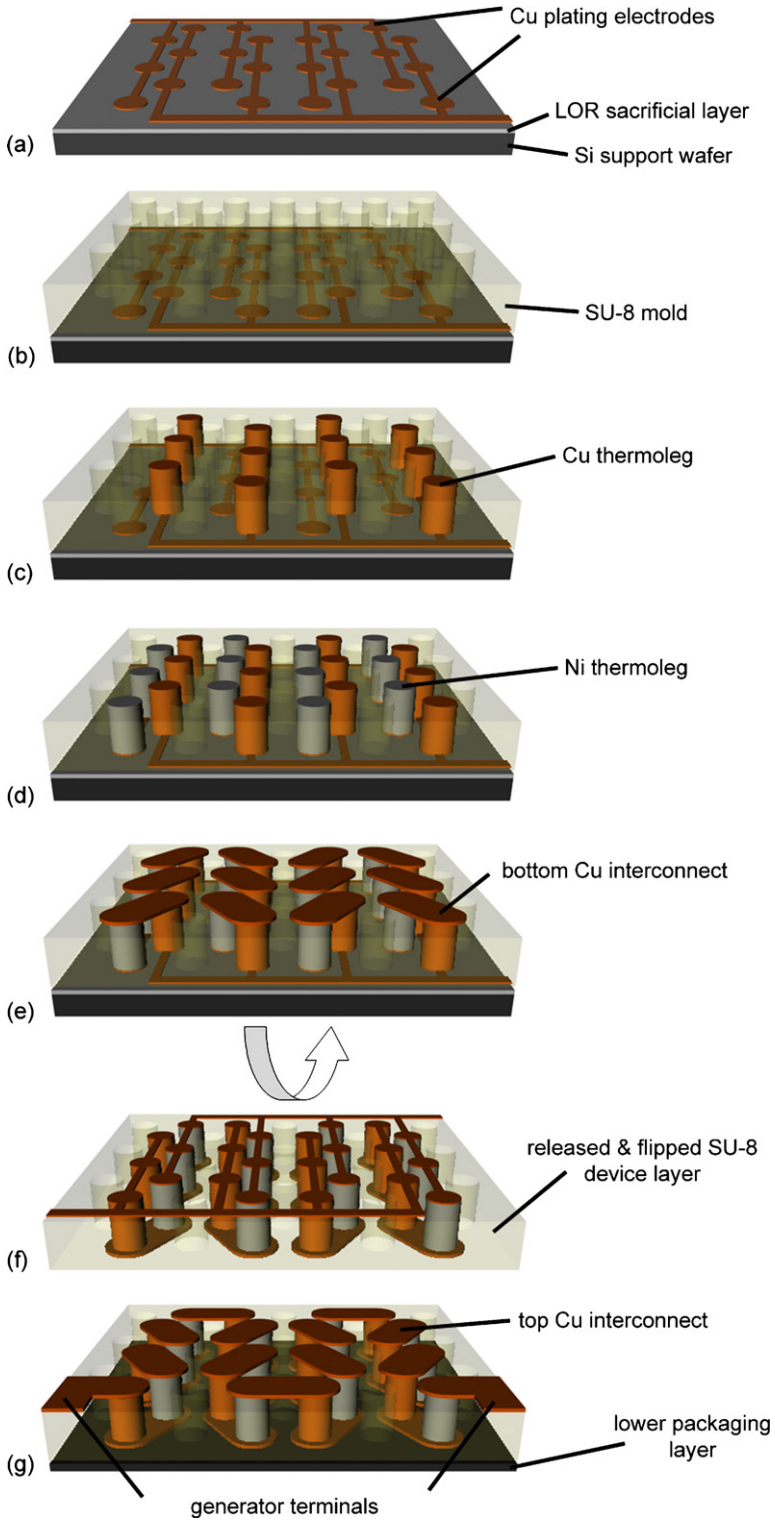

Fig. 8. Fabrication process for flexible μTEG. (a) Patterning of seed layer electrodes; (b) structuring of SU-8 mold; (c) selective ECD of Cu-thermolegs; (d) ECD of Ni-thermolegs; (e) the bottom interconnects between the different thermolegs are etched into a 20-μm thick electroplated Cu-layer; (f) release of SU-8 layer by removing the sacrificial layer. Flipping the SU-8 disk gives access to the plating electrodes; (g) patterning of top interconnects and bond pads. The SU-8 device layer is bonded onto a lower packaging layer. The device is completed after top interconnects are defined by etching a 20-μm thick electrochemically deposited Cu-layer. In this etching step the thin plating electrodes are removed as well.

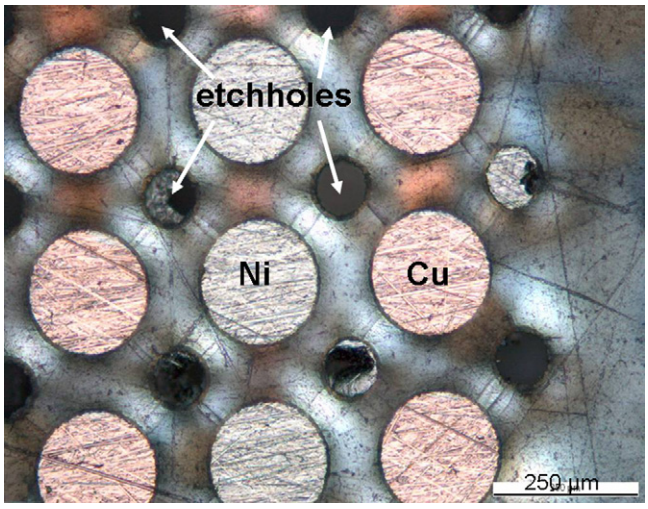

Fig. 9. Array of Cu- and Ni-thermolegs in a SU-8 mold after polishing.

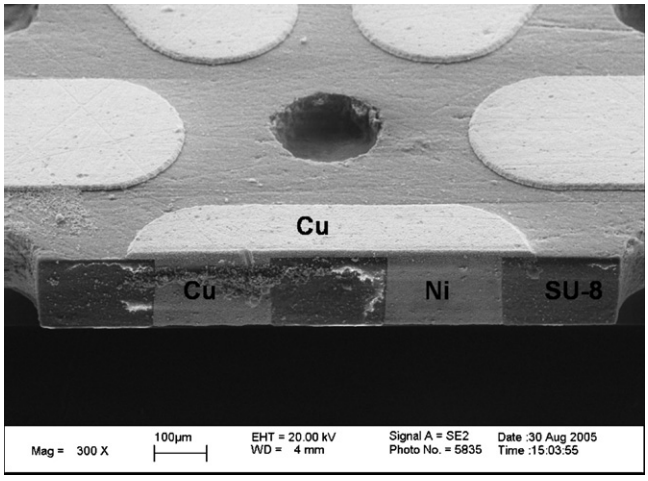

Fig. 10. SEM image of a cut through a Ni–Cu thermocouple connected by a 15 µm thick Cu interconnect on the top side shows void free electrochemical deposition.

layer with thermal glue or if an unpackaged device is preferred to a support wafer by means of a photo resist. Finally the device is finished by patterning the top interconnects by etching a 20-µm thick electrochemically deposited Cu-layer (Fig. 8g). In this etching step the thin plating electrodes are removed as well. First devices have been fabricated with this process. A µTEG with 90 Ni–Cu thermocouples on an area of 7 mm × 7 mm is depicted in Fig. 11. In this case the device has no additional packaging layer. The meander shape serial connection of the thermocouples is visible through the transparent SU-8.

4. Material properties

To verify the model by experiment the material properties need to be determined independently. Of the materials used for the generator the metals Cu and Ni are well characterized so the experimentally determined material properties can easily be compared and controlled with literature values. In contrast for SU-8 many properties have not been investigated thoroughly. In a first experiment the thermal conductivity of SU-8 was examined in a measurement setup where 20 mm × 20 mm test samples with a layer of SU-8 deposited on top of a silicon substrate are mounted between a temperature controlled cooler and a micromachined heater chip with integrated temperature sensors. The thermal resistance of the sample is determined by measuring the power supplied to the heater and the temperatures measured on the hot side of the sample after reaching equilibrium. All parasitic thermal resistances from the setup, the thermal contact grease and the substrate are eliminated by measuring samples of different thicknesses. The measurement yielded a thermal conductivity of $0.208 \pm 0.035\ \mathrm{W\,m^{-1}\,K^{-1}}$ for SU-8. According to the model the loss introduced by thermal conduction through the SU-8 for the presented demonstrator is 0.9%. Because of their limited thickness µTEGs are very sensitive to the quality of the thermal contacts to hot and cold side. The optimal length of the thermocouples varies significantly depending on the thermal

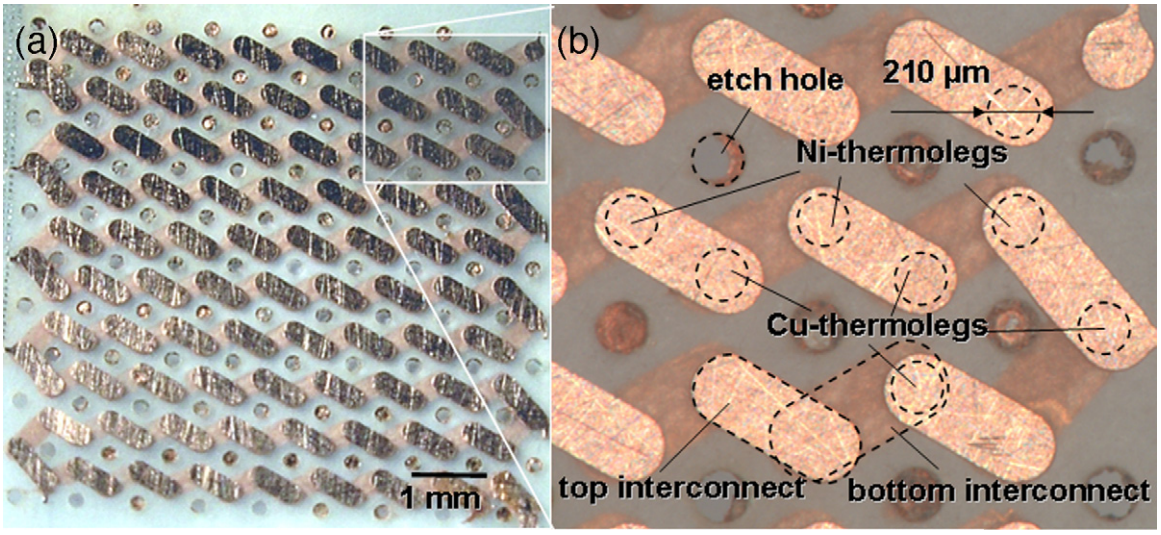

Fig. 11. Light microscopic images of thermoelectric generator device. (a) Complete device with 90 Cu–Ni thermocouples in a meander shape serial connection accordingly to Fig. 8g. Ninety-nine etch holes are collocated across the device. (b) Detailed cut out view. Bright Cu top interconnect and the darker trough shining bottom interconnects electrically connect all thermolegs in series. The diameter of the thermolegs and the etch holes is 210 µm.

Table 2
Comparison of different published micro thermoelectric generators with the demonstrator presented in this paper and a planed device of which the predicted performance was calculated with the introduced general model

	Group			
	Infineon	MicroPelt	ETH	
	Ref. [5]	Ref. [7]	Model	Demonstrator
Material/process	Bi-CMOS poly-Si thermocouples, microcavities for thermal insulation	Dry etched sputtered BiTe wafer soldered onto each other	Electroplating of BiTe TCs into polymer mold	Electroplating of Ni–Cu TCs into polymer mold
Thermocouple material	p–n poly-Si	p–n Bi_2Te_3	p–n Bi_2Te_3	Cu, Ni
Seebeck coefficient ($\mu V\,K^{-1}$)	160	~340	400	20.6
Thermal conductivity [$W\,m^{-1}\,K^{-1}$]	31		1.5	Cu, 401; Ni, 90.7
Specific resistance ($\Omega\,m$)			1×10^{-5}	Cu, 1.73×10^{-8}; Ni, 7.2×10^{-8}
Leg-length (μm)	18.5	20	110	150
Inactive/active area			1.5	6.3
Integration (TCs/cm^2)	225400	1080	2310	183
Specific contact resistance ($\Omega\,m^2$)	$\sim 9.3 \times 10^{-11}$	$\sim 5 \times 10^{-11}$	6.4×10^{-11}	6.4×10^{-11}
Internal resistance (Ω/cm^2)	29×10^6	~800	655	5.96
Efficiency factor ($\mu W\,K^{-2}\,cm^{-2}$)	0.0426 (poly-Si); 0.0352 (poly-SiGe)	65[a]	96	0.833

[a] Number was calculated from data given in the reference.

contact resistances and the material of the thermocouples. The optimum for Ni–Cu thermocouples would be a length of around 3 cm, which is out of range for a micromachining approach. But for the projects long term target design with thermocouples made of BiTe the optimal length is in the range of 110 μm, assuming thermal contact resistances on both sides of the device can be reduced to 1.0 K/W. Table 2 list all other material properties that are relevant for the introduced model. The listed values are taken from literature [3,11] and will be independently determined in later experiments.

5. Measurements

The fabricated devices are tested and characterized with the measurement setup depicted in Fig. 12. The temperature difference and range can be adjusted via two PID controller units driving a hot plate and a Peltier cooler, respectively. Fig. 13 shows the output power of the μTEG as function of the measured temperature difference. The tested device had 51 thermocouples with a height of 150 ± 10 μm on a surface of $0.26\,cm^2$. The internal resistance of the generator was $1.55 \pm 0.02\,\Omega$. This value corresponds to a low contact resistance between thermolegs and interconnects of $7.5 \times 10^{-3}\,\Omega$. The importance of low contact resistance may be directly derived from the thermoelectric model and from analyzing other groups' results as can be seen in Table 2. The experiment was recorded with a load resistance of $1.734 \pm 0.001\,\Omega$. The results were compared with the analytic model described above. The model accounts for thermal losses due to the thermal resistances $K_H = 6.5 \pm 0.2$ K/W and $K_C = 17.7 \pm 1.0$ K/W between the location of the tem-

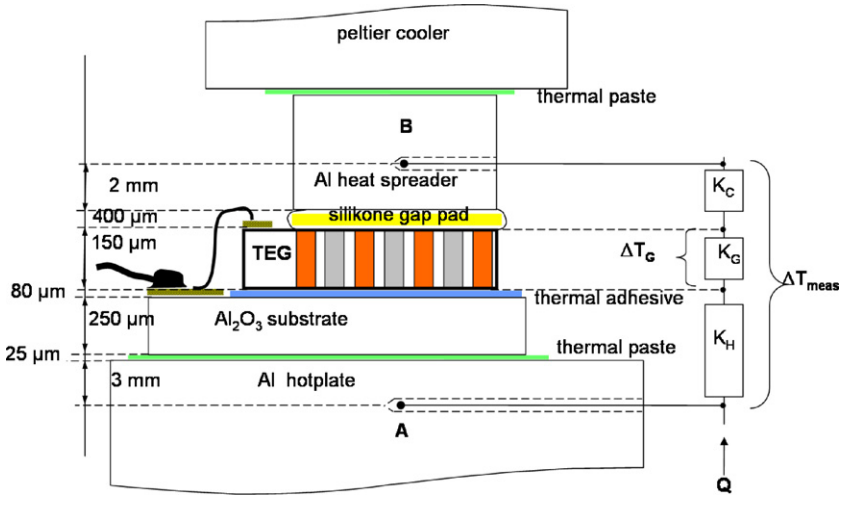

Fig. 12. Schematic of measurement set-up. The temperature difference ΔT_{meas} is measured between points A and B. The temperature difference across the thermoelectric generator ΔT_G is unknown but can be determined if the thermal resistances K_H, K_C, K_G are calculated from the geometry and the material parameters of the set-up and the device, respectively.

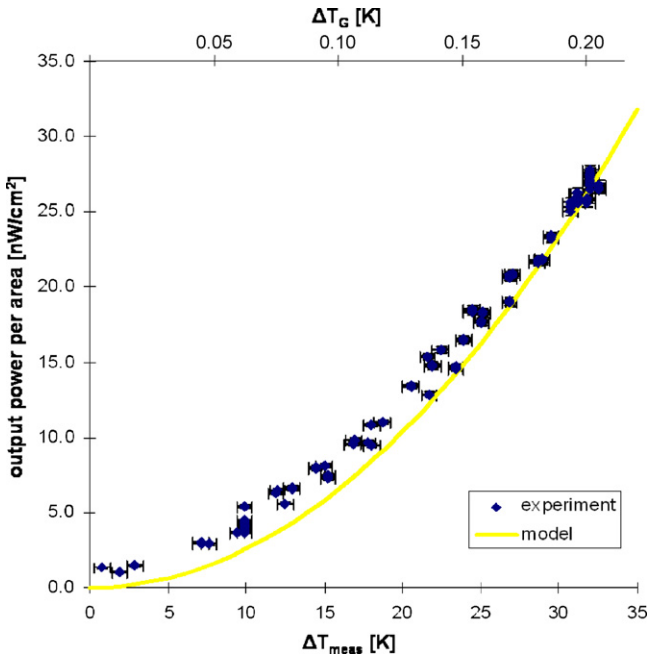

Fig. 13. Measured and calculated power output per area of thermoelectric generator in dependence of the measured temperature difference and the calculated temperature drop over the TEG according to Fig. 11. The offset at $\Delta T = 0$ K for the experimental result is due to the uncertain temperatures at the generator surfaces.

perature probes and the generator surface. These resistances are big compared to the thermal resistance of the generator $K_G = 0.17 \pm 0.02$ K/W so that the temperature difference over the device is by a factor of ~150 smaller for the given configuration. The model is in good accordance with the experiment. The μTEG generated a power of 12.0 ± 1.1 nW/cm^2 for a ΔT_{meas} of 20 K or ΔT_G of 0.12 K.

6. Conclusion

We have presented and analyzed a model for vertical μTEGs. According to the analysis the output power per area is independent of the number of the thermolegs and of their cross-sectional area. Instead it depends just on the ratio of the cross sectional areas of insulation and thermolegs and of the length of the thermolegs. The power shows a maximum for a certain thermocouple length depending on the other parameters. In the range around optimum performance the power per area increases when the above-mentioned ratio of insulation to active material is minimized. Hence the insulation area around the thermolegs should be minimized and the crossectional area of the thermoleg should be maximized keeping in mind the voltage need of the application and the area allocated for the generator. Larger cross sections of the thermolegs facilitate achieving low contact resistances which increases the power output. In addition the requirements for the photolithographic patterning are reduced yielding lower fabrication costs. For given material and interfaces the generator may be tuned to optimum performance through the leg length. Assuming BiTe thermocouples and realistic thermal interfaces the optimal leg length is in the range of 80–150 μm. We successfully demonstrated a new fully integrated process flow for low cost fabrication of flexible μTEGs in that range of thickness. First experimental results are in good accordance with the model. By replacing Ni–Cu thermocouples by electrochemically deposited BiTe [12] the generator performance may be pushed to 96 μW K^{-2} cm^{-2} as can be seen in Table 2. This table compares the TEGs of different groups to the demonstrator presented and a planned device for which the expected performance was calculated with the introduced model and the listed material parameters. Substituting SU-8 by another polymer may also increase flexibility if necessary for the application of μTEGs on surfaces with high curvature.

Acknowledgements

The authors would like to thank K. Vollmers for help with the electrochemical deposition, Dr. R. Linderman of the Zurich IBM Research Lab for help with the thermal conductivity measurements and A. Hutterli for help with the design. We would also thank the ETH Zürich for funding of this project.

References

[1] M. Kishi, H. Nemoto, T. Hamao, M. Yamamoto, S. Sudou, M. Mandai, S. Yamamoto, Micro thermoelectric modules and their application to wristwatches as an energy source, in: 18th International Conference on Thermoelectrics. Proceedings-ICT'99, Cat. No. 99TH8407, 1999, pp. 301–307.

[2] H. Glosch, M. Ashauer, U. Pfeiffer, W. Lang, A thermoelectric converter for energy supply [using silicon micromechanics], Sensors Actuators A: Phys. 20 (1999) 1–3.

[3] S. Hasebe, J. Ogawa, M. Shiozaki, T. Toriyama, S. Sugiyama, H. Ueno, K. Itoigawa, Polymer based smart flexible thermopile for power generation, in: 17th IEEE International Conference on Micro Electro Mechanical Systems. Maastricht MEMS 2004 Technical Digest (IEEE Cat. No. 04CH37517), 2004, pp. 689–692.

[4] I. Stark, M. Stordeur, New micro thermoelectric devices based on bismuth telluride-type thin solid films, in: 18th International Conference on Thermoelectrics. Proceedings-ICT'99, Cat. No. 99TH8407, 1999, pp. 465–472.

[5] M. Strasser, R. Aigner, C. Lauterbach, T.F. Sturm, M. Franosch, G. Wachutka, Micromachined CMOS thermoelectric generators as on-chip power supply, in: TRANSDUCERS, Solid-State Sensors, Actuators and Microsystems, 12th International Conference on, vol. 1, 2003, pp. 45–48.

[6] G.J. Snyder, J.R. Lim, C.K. Huang, J.P. Fleurial, Thermoelectric microdevice fabricated by a MEMS-like electrochemical process, Nat. Mater. 2 (2003) 528–531.

[7] H. Bottner, J. Nurnus, A. Gavrikov, G. Kuhner, M. Jagle, C. Kunzel, D. Eberhard, G. Plescher, A. Schubert, K.H. Schlereth, New thermoelectric components using microsystem technologies, J. Microelectromech. Syst. 13 (2004) 414–420.

[8] G. Min, D.M. Rowe, Peltier devices as generators, in: D.M. Rowe (Ed.), CRC Handbook of Thermoelectrics, CRC Press, London, 1995 (Chapter 38).

[9] V.A. Semenyuk, Advances in development of thermoelectric modules for cooling electro-optic components, in: Proceedings-ICT'03, 22nd International Conference on Thermoelectrics, 2003, pp. 631–636.

[10] V. Seidemann, S. Butefisch, S. Buttgenbach, Fabrication and investigation of in-plane compliant SU8 structures for MEMS and their application to micro valves and micro grippers, Sensors Actuators A: Phys. 97/98 (2002) 457–461.

[11] D.R. Lide (Ed.), CRC Handbook of Chemistry and Physics, CRC Press, 2003.
[12] M.S. Martin-Gonzalez, A.L. Prieto, R. Gronsky, T. Sands, A.M. Stacy, Insights into the electrodeposition of Bi_2Te_3, J. Electrochem. Soc. 149 (2002) C546–C554.

Biographies

Wulf Glatz received his diploma degree in Mechanical Engineering from the Technical University Braunschweig, Germany in 2002 specializing in Microsystems Technology. During his studies he conducted a project work on quartz crystal microbalances at the Polytechnic University of Valencia, Spain. His diploma thesis on quadrature compensation methods for silicon gyroscopes was carried out at the BOSCH Research Division. Currently, he is working as a PhD student within the Micro and Nanosystems group at ETH Zurich focusing on the development of micro thermoelectric generators.

Simon Muntwyler is currently studying Mechanical Engineering at ETH Zurich. He is focusing in micro and nanosystems as well as in control systems. Currently, he is finishing his studies towards a Dipl.-Ing. ETH degree.

Christofer Hierold is Professor for Micro- and Nanosystems at ETH Zurich since April 2002. Before, he was 11 years with Siemens AG, Corporate Research, and Infineon Technologies AG in Munich, Germany, working mainly on CMOS compatible microsystems. His major research at ETH Zurich is now focused on the field of nanotransducers, evaluation of new materials for MEMS and advanced microsystems. Christofer Hierold has been serving in program committees of numerous scientific conferences; he is member of the International Steering Committee for the European Conference on Solid-State Transducers (Eurosensors) and for the International Conference on Solid-State Sensors, Actuators and Microsystems (Transducers). He is active as subject editor of the IEEE/ASME Journal of Micro Electromechanical Systems, JMEMS, and as joint editor of Wiley-VCH's book series on "Advanced Micro and Nanosystems".